Journal of Turbulence

ISSN: (Print) 1468-5248 (Online) Journal homepage: http://www.tandfonline.com/loi/tjot20

Grid and subgrid-scale interactions in viscoelastic turbulent flow and implications for modelling

M. Masoudian, C.B. da Silva & F.T. Pinho

To cite this article: M. Masoudian, C.B. da Silva & F.T. Pinho (2016) Grid and subgrid-scale interactions in viscoelastic turbulent flow and implications for modelling, Journal of Turbulence, 17:6, 543-571, DOI: 10.1080/14685248.2015.1125492

To link to this article: http://dx.doi.org/10.1080/14685248.2015.1125492

JOURNAL OF TURBULENCE, 2016
VOL. 17, NO. 6, 543–571
http://dx.doi.org/10.1080/14685248.2015.1125492

Taylor & Francis
Taylor & Francis Group

Grid and subgrid-scale interactions in viscoelastic turbulent flow and implications for modelling

M. Masoudian[a], C.B. da Silva[b] and F.T. Pinho[a]

[a]Transport Phenomena Research Center, Faculty of Engineering, University of Porto, Rua Dr. Roberto Frias s/n, 4200-465 Porto, Portugal; [b]IDMEC, Instituto Superior Técnico, Universidade de Lisboa, Pav. Mecanica I, LASEF, Av. Rovisco Pais, 1049-001 Lisboa, Portugal

ABSTRACT

Using direct numerical simulations of turbulent plane channel flow of homogeneous polymer solutions, described by the Finitely Extensible Nonlinear Elastic-Peterlin (FENE-P) rheological constitutive model, a-priori analyses of the filtered momentum and FENE-P constitutive equations are performed. The influence of the polymer additives on the subgrid-scale (SGS) energy is evaluated by comparing the Newtonian and the viscoelastic flows, and a severe suppression of SGS stresses and energy is observed in the viscoelastic flow. All the terms of the transport equation of the SGS kinetic energy for FENE-P fluids are analysed, and an approximated version of this equation for use in future large eddy simulation closures is suggested. The terms responsible for kinetic energy transfer between grid-scale (GS) and SGS energy (split into forward/backward energy transfer) are evaluated in the presence of polymers. It is observed that the probability and intensity of forward scatter events tend to decrease in the presence of polymers.

ARTICLE HISTORY
Received 15 May 2015
Accepted 21 November 2015

KEYWORDS
Direct numerical simulation; polymer drag reduction; large eddy simulation; turbulence modelling: subgrid-scale; small scale intermittency

1. Introduction

In 1949, Toms [1] observed experimentally that the addition of small amounts of polymer to Newtonian turbulent flows can severely reduce the turbulent friction drag by up to 80%. Over the last decades, the development of accurate and efficient numerical and experimental methods has made it possible to investigate the mechanism of drag reduction in detail.[2–5] Amongst others, two different explanations for this mechanism were postulated by Lumley [6] and Tabor and de Gennes.[7] Lumley [6] related the mechanism of drag reduction by polymer additives to the polymer chains extension, suggesting that in the buffer layer, where strong deformations occurs, the stretching of coiled polymers increases the effective extensional viscosity thereby further dissipating small scale eddies, which thickens the viscous sublayer and consequently leads to drag reduction. Tabor and de Gennes [7] studied the drag reduction by polymer additives in the context of homogeneous isotropic turbulence, and related drag reduction to storage and release of energy by the polymer molecules.

CONTACT M. Masoudian mmasoudian@fe.up.pt

Several direct numerical simulation (DNS) investigations of fully developed turbulent channel and pipe flow have been carried out to understand the effect of rheological parameters on the structure of turbulence and turbulence statistics. Extensive results about the influence of rheological parameters on the amount of drag reduction have been reported in [8,9]. These authors used the Finitely Extensible Nonlinear Elastic-Peterlin (FENE-P) and Giesekus constitutive equations to investigate the effects of polymer relaxation time, chain extensibility, and polymer to solution viscosity ratio on the turbulent flow characteristics.

DNS of turbulent viscoelastic flows has shed light on the mechanism and different aspects of drag reduction (DR) by polymer additives over the last two decades; however, the DNS of the turbulent flows with homogenous polymer additives is much more expensive than the corresponding Newtonian turbulent flow, because the constitutive equation increase the number of primary variables, and these extra equations must be solved to account for the polymer contribution. Moreover, as DR increases, the near wall streaks become progressively stabilised and elongated, thus requiring the use of longer simulation boxes in particular for high DR cases.[8] Consequently, for a given Reynolds number, the CPU time and memory requirements for DNS of viscoelastic flows are at least one order of magnitude larger than for the corresponding Newtonian case, which is unfeasible for engineering applications. Hence, large eddy simulation (LES) and Reynolds-averaged Navier–Stokes (RANS) models need to be developed for modelling turbulent flows of dilute polymer solutions for engineering applications.

In the context of RANS models for FENE-P fluids Iaccarino et al.,[10] and Masoudian et al. [11] developed $k - \varepsilon - \overline{v^2} - f$ models for FENE-P fluids. These models are fairly simple, introducing the concept of turbulent polymer viscosity to calculate various time averaged quantities. However, the quantitative information about turbulence from RANS is limited because of the inherent nature of RANS.

In order to cope with the high computational cost of DNS and the limitation of RANS models, LES of turbulent flows of viscoelastic fluids need to be developed in order to allow carrying out numerical simulations for engineering applications. The first attempts at LES of turbulent drag-reducing channel flow of viscoelastic fluids was carried out by Thais et al. [12] in the context of temporal large eddy simulation. Using this method, they were able to predict all turbulence statistics. More recently, Wang et al. [13] performed LES of forced homogeneous isotropic turbulence of FENE-P fluids using the temporal approximate de-convolution method, and investigated the characteristics of turbulence structures and statistics.

Recently, Ohta et al. [14] developed a modified Smagorinsky model for turbulent channel flow of generalised Newtonian fluids, with viscosity described by the power-law model, and focused on low-Reynolds-number wall turbulence of non-Newtonian inelastic fluids.

Presently, subgrid-scale (SGS) models for large eddy simulations of turbulent drag-reducing flows with additives described by differential viscoelastic constitutive equations, such as the FENE-P models, are rare. This work is precisely motivated by the need to understand the effect of viscoelasticity on the filtered governing equations arising in LES. For this purpose, DNSs of turbulent channel flow of FENE-P fluids were carried out. In this work, a top filter is used to separate the grid scales (GS) and SGS. The additional terms appearing in the momentum equation for FENE-P fluids due to the filtering procedure are then

calculated and the influence of rheological parameters is investigated. Additionally, the filtered FENE-P constitutive equation is also investigated and the resolved and unresolved terms are identified and assessed.

As stressed by [15–17] in the context of Newtonian turbulent flows, accurate modelling of the direct and inverse energy transfer between GS and SGS is crucial, particularly for non-equilibrium flows. Although this issue has received attention for Newtonian fluids, no effort has actually been made to quantify this phenomenon in turbulent drag reducing flows described by the FENE-P constitutive equation, particularly in wall bounded flows. In this work, we analyse for the first time the backward and forward scatter behaviour of the terms incorporating the GS/SGS energy transfer by using the SGS kinetic energy transport equation appropriate for FENE-P fluids.

The organisation of this paper is as follows. In the next section, the governing equations for FENE-P fluids and the numerical methods used in the DNSs will be presented. In Section 3, the DNS data will be assessed. In Section 4, the results will be presented and discussed, and finally the conclusions will be summarised in Section 5.

2. Governing equations and numerical method

2.1. Governing equations

Figure 1 shows a schematic of the channel flow studied in this work, where the x-axis is chosen as the mean flow direction, and the y- and the z-axes are the wall-normal and spanwise directions, respectively. The conservation of mass and momentum equations appropriate for FENE-P fluid are

$$\nabla . \overrightarrow{u} = 0, \tag{1}$$

$$\frac{\partial \overrightarrow{u}}{\partial t} + \overrightarrow{u} . \nabla \overrightarrow{u} = -\nabla p + \frac{1}{\mathrm{Re}_{\tau 0}} \left[\beta \nabla^2 \overrightarrow{u} + (1-\beta) \nabla . \overline{\overline{\tau}}_v \right], \tag{2}$$

where $\overrightarrow{u}$, p, and $\overline{\overline{\tau}}_v$ denote the instantaneous velocity vector, pressure, and viscoelastic tensor contribution to the total extra stress tensor, respectively. The zero shear rate friction Reynolds number, $Re_{\tau 0}$, is defined as $Re_{\tau 0} = hU_\tau/\nu_0$, where ν_0 is the zero shear rate kinematic viscosity of the solution, U_τ is the friction velocity, $U_\tau = (\tau_w/\rho)^{1/2}$, and h is the half-height of the channel, that together with the time scale, h/U_τ, are utilised to normalise

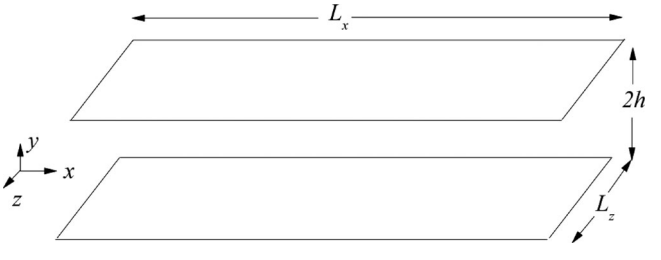

Figure 1. Schematic of the flow geometry, x: streamwise, y: wall normal, and z: spanwise directions.

the equations. The parameter β is the ratio of the solvent to the total solution zero shear-rate viscosity, $\beta = \nu_s/\nu_0$.

The additional viscoelastic stress tensor ($\overline{\overline{\tau}}_v$) in Equation (2) arises due to the presence of polymer. The stress tensor for the FENE-P dumbbells is given by

$$\overline{\overline{\tau}}_v = \frac{f(c_{kk})\overline{\overline{c}} - I}{Wi_h}, \tag{3}$$

where $Wi_h = \lambda U_\tau/h = Wi_{\tau 0}/Re_{\tau 0}$, is the dimensionless relaxation time, also known as Weissenberg number, $\overline{\overline{c}}$ is the conformation tensor, which quantifies the normalised second moment of the dumbbell end-to-end distance vector, and I is the identity matrix. Function $f(c_{kk})$ is known as the Peterlin function defined by

$$f(c_{kk}) = \frac{L^2}{L^2 - c_{kk}}. \tag{4}$$

Note that $\overline{\overline{c}}$ and L^2 are made dimensionless with respect to k_BT/H^*, where k_B, T, and H^* denote the Boltzmann constant, the absolute temperature, and the Hookean dumbbell spring constant, respectively. The polymer conformation tensor is obtained by solving the following evolution equation for the dimensionless conformation tensor,

$$\frac{\partial \overline{\overline{c}}}{\partial t} + \overrightarrow{u} \,.\nabla \overline{\overline{c}} - \left[\overline{\overline{c}}.\nabla \overrightarrow{u} + (\nabla \overrightarrow{u})^T.\overline{\overline{c}}\right] - D\nabla^2\overline{\overline{c}} = -\overline{\overline{\tau_v}}. \tag{5}$$

2.2. Filtering procedure

In LES, all variables of the flow (φ) are decomposed into a GS ($\varphi^<$) and a SGS part ($\varphi^>$). Using this notation, the main flow variables are decomposed as

$$u_i = u_i^< + u_i^>,\ p = p^< + p^>,\ \tau_{v,ij} = \tau_{v,ij}^< + \tau_{v,ij}^>,$$

where the GS are identified by

$$\varphi^<(x) = \int_\Omega \varphi(x')\, G_\Delta(x - x')dx. \tag{6}$$

In this equation, $G_\Delta(x)$ is the filter kernel of width Δ, which must satisfy $\int_\Omega G_\Delta(x)dx = 1$, $\varphi(x)$ is a given flow variable, and the integration is extended over the entire flow domain, Ω.

In a-priori tests, the resolved velocity fields obtained from DNS are explicitly filtered in order to obtain the exact quantities of interest. The filter kernel that is used here is the box or top-hat filter defined as

$$G(x) = \begin{cases} 1/\Delta & \text{if } |x| \le \Delta/2 \\ 0 & \text{otherwise} \end{cases}. \tag{7}$$

2.2.1. Filtered Navier–Stokes equation

Applying the filtering operation to the continuity and Navier–Stokes equations yields the so-called filtered Navier–Stokes equations, which govern the evolution of the GS of motion

$$\frac{\partial u_i^<}{\partial t} + \frac{\partial u_i^< u_j^<}{\partial x_j} = -\frac{\partial p^<}{\partial x_i} + \frac{\beta}{\mathrm{Re}_{\tau 0}} \frac{\partial}{\partial x_j}\left(\frac{\partial u_i^<}{\partial x_j} + \frac{\partial u_j^<}{\partial x_i}\right) - \frac{\partial \tau_{ij}}{\partial x_j} + (1-\beta)\frac{\partial \tau_{v,ij}^<}{\partial x_j}, \tag{8}$$

$$\frac{\partial u_i^<}{\partial x_i} = 0, \tag{9}$$

where τ_{ij} is the unknown subgrid-stress tensor defined by $\tau_{ij} = (u_i u_j)^< - u_i^< u_j^<$, which quantifies the momentum exchanges between the grid and subgrid scales, and it needs to be modelled in LES.

2.2.2. Filtered conformation tensor equation

The last term on the right-hand side of the filtered Navier–Stokes equation is the filtered polymer extra stress tensor which arises by filtering Navier–Stokes equation for FENE-P fluids, and can be expressed as

$$\tau^<_{ij,v} = \frac{\eta_p}{\lambda}\left[f(c_{kk})c_{ij} - f(L)\delta_{ij}\right]^< = \frac{\eta_p}{\lambda}\left(f(c_{kk})c_{ij}\right)^< - \frac{\eta_p}{\lambda} f(L)\delta_{ij}\,. \tag{10}$$

By applying the filtering operation described above, the filtered FENE-P constitutive equation is obtained

$$\frac{\partial c_{ij}^<}{\partial t} + u_k^< \frac{\partial c_{ij}^<}{\partial x_k} - \left(c_{ik}^< \frac{\partial u_j^<}{\partial x_k} + c_{jk}^< \frac{\partial u_i^<}{\partial x_k}\right) + \frac{\tau_{ij,v}^<}{\eta_p} = FT_{ij} + ST_{ij}\,, \tag{11}$$

where the two terms on the right-hand side include the following SGS contributions:

$$FT_{ij} = u_k^< \frac{\partial c_{ij}^<}{\partial x_k} - \left(u_k \frac{\partial c_{ij}}{\partial x_k}\right)^<,$$

and

$$ST_{ij} = \left(c_{ik}\frac{\partial u_j}{\partial x_k} + c_{jk}\frac{\partial u_i}{\partial x_k}\right)^< - \left(c_{ik}^< \frac{\partial u_j^<}{\partial x_k} + c_{jk}^< \frac{\partial u_i^<}{\partial x_k}\right),$$

where FT_{ij} and ST_{ij} are unknown terms representing grid/subgrid-scale interactions in the FENE-P constitutive equation.

2.2.3. Transport equations for the grid-scale and subgrid-scale kinetic energy

In order to study the interaction between GS and SGS kinetic energies, the equations governing these quantities in a viscoelastic turbulent channel flow will be analysed. The transport equation for (twice) the GS kinetic energy ($k = \frac{1}{2}u_i^< u_i^<$) for viscoelastic fluids

described by the FENE-P model is given by

$$\underbrace{\frac{\partial u_i^{<} u_i^{<}}{\partial t}}_{\text{(A)}} + \underbrace{\frac{\partial u_i^{<} u_i^{<} u_j^{<}}{\partial x_j}}_{\text{(B)}} = -2\underbrace{\frac{\partial p^{<} u_i^{<}}{\partial x_i}}_{\text{(C)}} + \underbrace{\frac{\beta}{\mathrm{Re}_\tau}\frac{\partial}{\partial x_j}\left(\frac{\partial k}{\partial x_j}\right)}_{\text{(D)}} \underbrace{-\frac{2\beta}{\mathrm{Re}_\tau}\frac{\partial u_i^{<}}{\partial x_j}\frac{\partial u_i^{<}}{\partial x_j}}_{\text{(E)}}$$
$$\underbrace{-2\frac{\partial \tau_{ij} u_i^{<}}{\partial x_j}}_{\text{(F)}} + \underbrace{2\tau_{ij} S_{ij}^{<}}_{\text{(G)}} + \underbrace{2(1-\beta)\frac{\partial \tau_{v,ij}^{<} u_i^{<}}{\partial x_j}}_{\text{(H)}} \underbrace{-2(1-\beta)\tau_{v,ij}^{<} S_{ij}^{<}}_{\text{(I)}}. \quad (12)$$

It is important to recall the physical meaning of this equation and its respective terms. Terms A and B account for the total (local and advection) variation of GS kinetic energy, respectively. Terms C and D represent the diffusion of GS kinetic energy by pressure/velocity interactions and molecular viscosity, respectively. Term E is the local GS kinetic energy dissipation associated to the molecular viscosity. The terms F and G are the only terms involving the subgrid-stress tensor τ_{ij} and they are directly related to the kinetic energy exchanges between GS and SGS. Term F (GS/SGS diffusion) represents a diffusion of GS kinetic energy by interactions between the GS velocity and the SGS stresses. The GS/SGS transfer (term G), also called SGS dissipation, represents the transfer of kinetic energy between GS and SGS. Terms H and I account for the interactions between GS and polymer. Term H is hereafter called GS/Polymer diffusion, and term I is the GS/Polymer dissipation.

The transport equation for (twice) the SGS kinetic energy is given by

$$\underbrace{\frac{\partial \tau_{ii}}{\partial t}}_{\text{(J)}} + \underbrace{\frac{\partial \tau_{ii} u_j^{<}}{\partial x_j}}_{\text{(K)}} = \underbrace{\frac{\partial}{\partial x_j}\left(\left(u_i u_i\right)^{<} u_j^{<} - \left(u_i u_i u_j\right)^{<}\right)}_{\text{(L)}} \underbrace{-2\frac{\partial}{\partial x_i}\left(p^{<} u_i^{<} - \left(p u_i\right)^{<}\right)}_{\text{(M)}}$$
$$+ \underbrace{\frac{\beta}{\mathrm{Re}_\tau}\frac{\partial}{\partial x_j}\left(\frac{\partial \tau_{ii}}{\partial x_j}\right)}_{\text{(N)}} \underbrace{-\frac{2\beta}{\mathrm{Re}_\tau}\left(\left(\frac{\partial u_i}{\partial x_j}\frac{\partial u_i}{\partial x_j}\right)^{<} - \frac{\partial u_i^{<}}{\partial x_j}\frac{\partial u_i^{<}}{\partial x_j}\right)}_{\text{(O)}} + \underbrace{2\frac{\partial \tau_{ij} u_i^{<}}{\partial x_j}}_{\text{(P)}} \underbrace{-2\tau_{ij} S_{ij}^{<}}_{\text{(Q)}}$$
$$+ \underbrace{2(1-\beta)\frac{\partial\left(\tau_{v,ij} u_i\right)^{<}}{\partial x_j}}_{\text{(R)}} \underbrace{-2(1-\beta)\frac{\partial \tau_{v,ij}^{<} u_i^{<}}{\partial x_j}}_{\text{(S)}} \underbrace{-2(1-\beta)\left(\tau_{v,ij} S_{ij}\right)^{<}}_{\text{(T)}} + \underbrace{2(1-\beta)\tau_{v,ij}^{<} S_{ij}^{<}}_{\text{(U)}}. \quad (13)$$

Equation 13 expresses the mechanisms governing the evolution of (twice) the unresolved or SGS kinetic energy, in which terms J and K represent the local and advective variation of the SGS kinetic energy, respectively. The diffusion caused by the turbulence fluctuations of SGS kinetic energy is represented by term L (SGS turbulent transport), term M represents the SGS pressure/velocity interactions and term N accounts for the SGS viscous diffusion. Term O is the SGS viscous dissipation, while terms P and Q are the only terms involving the subgrid-stress tensor τ_{ij} and are directly related to the kinetic energy exchanges between GS and SGS. These two terms represent the classical kinetic energy cascade, which also exists in viscoelastic turbulent flows. Term P (GS/SGS diffusion) represents a redistribution of SGS kinetic energy by interactions between the GS velocity and the SGS stresses,

whereas the GS/SGS transfer (term Q) also often named SGS dissipation represents the transfer of kinetic energy between GS and SGS. It is important to notice that terms P and Q are, respectively, the symmetric of terms F and G appearing in the GS equation. Since these terms appear in both equations with opposite signs, they represent the kinetic energy exchange between GS and SGS. Although the same happens mathematically with viscoelastic terms H, I, S and U, respectively, here the transfer of energy between GS and SGS is carried out through GS/polymer and SGS/polymer interactions. If term Q is positive, the kinetic energy cascades from GS to SGS (forward scatter), otherwise SGS kinetic energy flows into the GS (backward scatter). As can be assessed by these equations, in the presence of polymer additives four new mechanisms must be accounted to study the GS/SGS interactions, which are absent in Newtonian flows. These are represented by terms R, S, T, and U. Term R represents additional diffusion prompted by polymer/velocity interactions, and at the end it does not involve net GS/SGS energy exchanges. This contrasts with term S, which also represents a diffusion prompted by the polymer, but involves a net GS/SGS energy exchange even if intermediated by the polymer. Terms T and U are similar to terms R and S, respectively, but are associated with source/sinks prompted by the polymer. Term T does not involve net energy exchange between GS and SGS, while term U does indeed involve kinetic energy exchanges between GS and SGS induced by the polymers in the solution. As with terms P and Q, positive values for terms U and S imply forward scatter, whereas negative values describe backward scatter events.

2.3. Numerical methods and fluid properties

The numerical algorithm proposed by [18] is used to carry out DNSs of turbulent channel flows. The algorithm relies on a semi-implicit spectral technique with periodic boundary conditions applied along the streamwise and spanwise directions. The channel sizes are equal to the sizes used in [8] to adequately capture the streaky structures and the elongated vortical structures arising in the turbulent flow. For the spatial discretisation in the two periodic directions (x, z), Fourier representations were used, whereas a Chebyshev approximation in the non-homogeneous shear direction was employed.

Note that, as demonstrated in [8,19], for low drag reduction (LDR), the temporal averaging is performed over 10–15 computational units (h/U_τ), whereas a much longer temporal averaging period of over 30–50 h/U_τ is required to obtain converged statistics for high drag reduction (HDR) flow due to the significant variations in xz plane.

The numerical integration of the evolution equation for the conformation tensor in turbulent channel flows relies on the use of a numerical diffusivity (term $D\nabla^2 c$) as described in [18,20,21], where D is a dimensionless number (equivalent to the inverse of a Schmidt number) defined as $D = \kappa/hU_\tau$, where κ denotes a constant isotropic artificial numerical diffusivity coefficient. This additional numerical diffusivity is small enough so that it does not affect the physics of the FENE-P model, and the corresponding computational results, while ensuring the numerical stability and realisability of the conformation tensor.[8,19] As in earlier studies,[8] the artificial numerical diffusivity D was taken to be of $O(10^{-2})$ resulting in a numerical Schmidt number $\mathrm{Sc}^+ = 1/Re_{\tau 0}D$ of the order of $O(10^{-1})$.

Note that the solvent and polymer stress fields are fully characterised by four dimensionless groups, namely, Re_τ, β, L^2, and Wi_τ. Table 1 summarises the computational parameters for the simulations carried out in this work.

Table 1. Summary of the physical and computational parameters for the DNS cases used in this work.

Case	$Re_{\tau 0}$	u_τ	Domain size $L_x \times L_y \times L_z$	Grid size n_x, n_y, n_z	L^2	$Wi_{\tau 0}$	β	DR
DNS0	395	0.000395	14.136h × 2h × 4.5h	384 × 257 × 192	0	0	0	0%
DNS1	395	0.000395	14.136h × 2h × 4.5h	384 × 257 × 192	3600	50	0.9	37%
DNS2	395	0.000395	14.136h × 2h × 4.5h	384 × 257 × 192	10000	100	0.9	55%

3. Flow statistics and DNS assessment

Streamwise mean velocity profiles in wall units for the cases described in Table 1 are shown in Figure 2. For the sake of comparison, the profiles for Virk's asymptote [22] (red solid line) and the Newtonian DNS data are also included. For the Newtonian case (DNS0), excellent agreement with the linear distribution in the viscous sublayer as well as in the logarithmic region is observed. In the drag reduced flows, it can be seen that all profiles in the viscous sub-layer also collapse on the linear distribution $U^+ = y^+$. Since the simulations are performed with a constant pressure gradient, drag reduction is manifested via an increase in the flow rate, hence further away from the wall the mean velocity of the drag reduced flows increases as compared to that in Newtonian flows, and the logarithmic profile is shifted upwards parallel to that of the Newtonian flow. The upward shift of the logarithmic profile is synonymous to drag reduction and can be interpreted as a thickening of the buffer layer.[6] Similar behaviour to the one described here was also found in the mean streamwise velocity profile in the channel flow experiments of Ptasinski et al. [23] and in earlier DNS studies.[8]

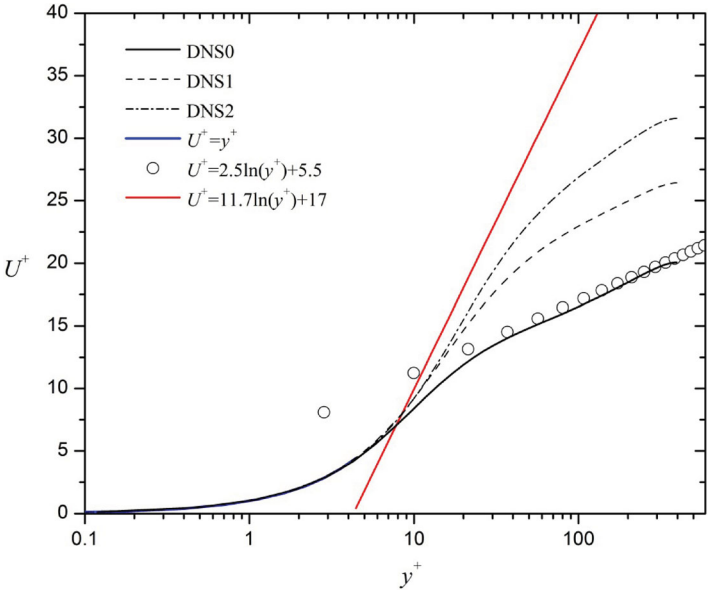

Figure 2. Mean streamwise velocity profiles as a function of distance from the wall for the DNSs used in this work (Table 1).

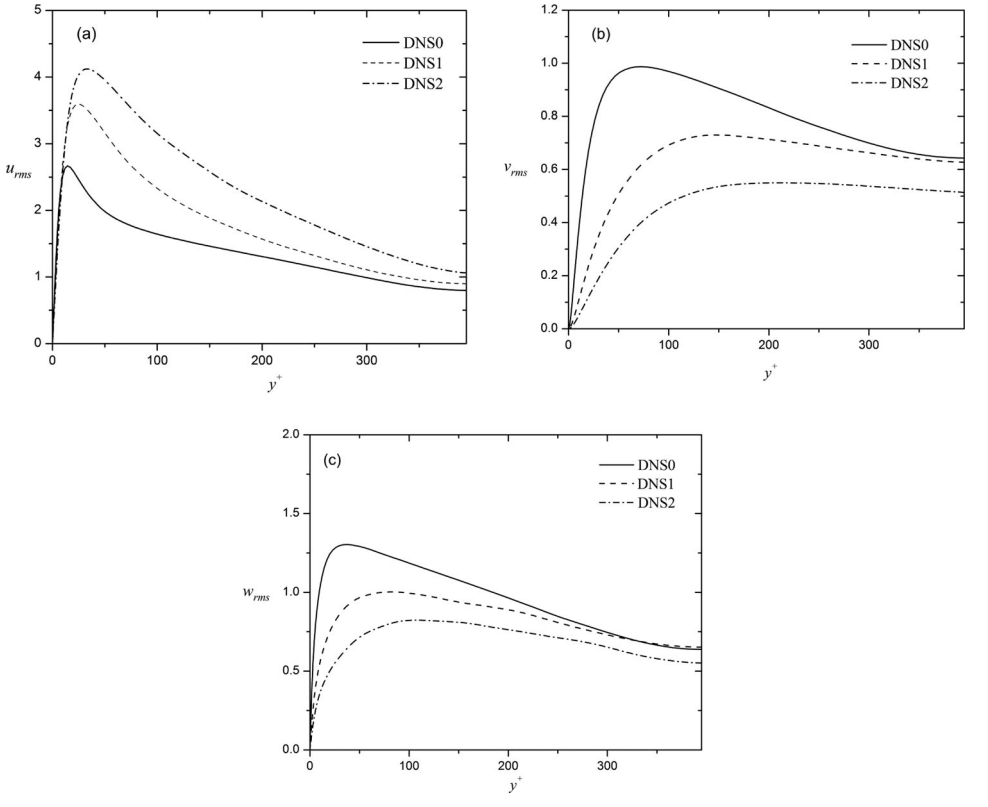

Figure 3. Root mean square of the velocity fluctuations for the DNSs used in this work (Table 1): (a) streamwise, (b) wall normal, and (c) spanwise components.

The corresponding transverse profiles of the root mean square of the streamwise velocity fluctuations for viscoelastic and Newtonian cases listed in Table 1 are shown in Figure 3(a). As is well known [8], the streamwise velocity fluctuations u_{rms} monotonically increase with increasing drag reduction. Simultaneously, the peak location of u_{rms} moves away from the wall as drag reduction increases, a behaviour that is consistent with the shift of the logarithmic region in the mean velocity profile. The wall normal and spanwise components of velocity fluctuations, v_{rms} and w_{rms}, are depicted in Figures 3(b) and 3(c), respectively. They show that v_{rms} and w_{rms} monotonically decrease as DR is increased, with the peak values of v_{rms} and w_{rms} also decreasing to almost half of their corresponding Newtonian values. Furthermore, the location of maxima of v_{rms} and w_{rms} also shifts away from the wall as drag reduction increases. All these results are consistent with previous experimental and numerical findings.[23]

In Figures 4(a)–4(c), the various contributions to the total shear stresses as a function of the distance from the wall are shown for the DNS0, DNS1, and DNS2 cases, respectively. In all cases, the total shear stresses follows the expected linear profiles over the channel height, indicating that the stationary fully developed state has been reached (for all cases in Table 1, this behaviour was checked). The figures indicate that for cases DNS1 and DNS2, low and high drag reduction, respectively, the polymer stress contribution increases monotonically with increasing DR, while the Reynolds stresses decrease. The polymer stress contribution

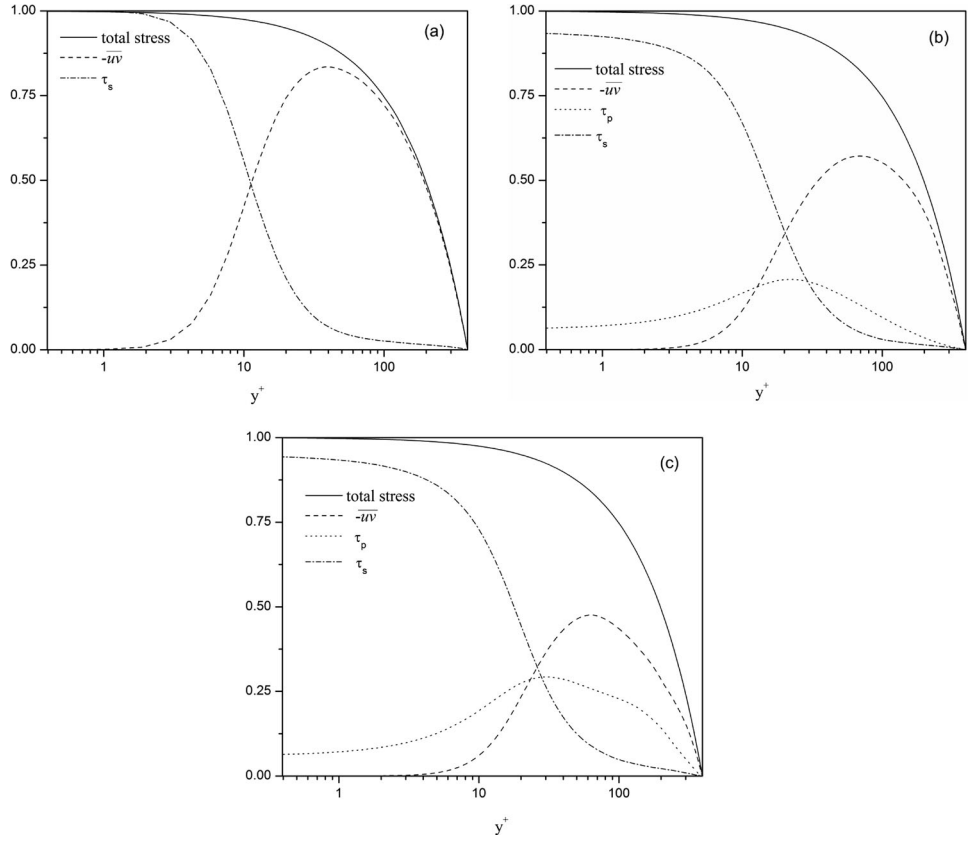

Figure 4. Total, Reynolds, solvent, and polymeric stresses for the DNSs used in this work (Table 1): (a) case DNS0, (b) case DNS1, (c) case DNS2, rheological and flow properties are described in Table 1.

is relatively small for low drag reduction (DNS1) and the location of the maximum is close to the wall, within the buffer layer. However, as DR increases, the Reynolds shear stress is significantly reduced, and the polymer stresses correspondingly increase, in agreement with the experimental results of [23]. In conclusion, the DNS data is consistent and over the next section will be used to investigate the GS–SGS interactions in viscoelastic turbulent channel flow.

4. Results and discussions

In this section, we analyse the grid/subgrid-scale interactions in turbulent channel flows with viscoelastic properties described in Table 1. The separation between grid and subgrid scales is achieved through the application of a box filter, with filter sizes equal to $4\Delta x_i$, $6\Delta x_i$, and $8\Delta x_i$ (these filter sizes are reported in Table 2 in terms of viscous length). Figure 5 shows the filtering procedure, where dashed lines represent the coarse grid filter, and the solid lines represent the DNS grid. The filters used in this work are applied in all three directions in such a way that the coarse grid, which has the size of filter (dashed line in Figure 5), was applied in the DNS domain, and the filtered quantity of interest at a specific point (for example point a in Figure 5) is equal to the mean value of the DNS points inside

Table 2. Filter sizes used in this work in viscous units.

Filter size	x^+	y^+	z^+
$4\Delta x_i$	58.163	$0.268 < y^+ < 14.5$	37.031
$6\Delta x_i$	87.245	$0.743 < y^+ < 24.2$	55.546
$8\Delta x_i$	116.327	$1.456 < y^+ < 33.9$	74.062

the course grid. For points in the vicinity of walls (point b in Figure 5), the averaging is performed over the available DNS data.

Note that, the averaged ratio of the SGS to GS kinetic energy for all chosen filter sizes are below 30% which indicates that all chosen filter sizes are representative of actual LES calculations.[15] Furthermore, all the conclusions and findings in this work were checked for all three filter sizes.

4.1. Subgrid-scale terms in the momentum and conformation tensor equations

The subgrid-stress tensor, τ_{ij}, in the momentum equation is responsible for the momentum exchanges between the grid and subgrid scales. Most SGS models are based on an artificial eddy viscosity approach, where the effects of the SGS turbulence are lumped into a turbulent or eddy viscosity as

$$\tau_{ij} - \frac{1}{3}\tau_{kk}\delta_{ij} = -2\upsilon_T S^<_{ij}, \tag{14}$$

where υ_T is the turbulent eddy viscosity and $S^<_{ij}$ is the large-scale rate of strain tensor. For instance, in the Smagorinsky model, one assumes that the turbulent eddy viscosity is proportional to the rate of strain norm, $|S^<| = \sqrt{2(S^<_{ij}S^<_{ij})}$. In order to analyse the influence of viscoelasticity on the subgrid stresses tensor, the quantity $\tau_{xy}/(-S^<_{xy}|S^<|)$, which is equal

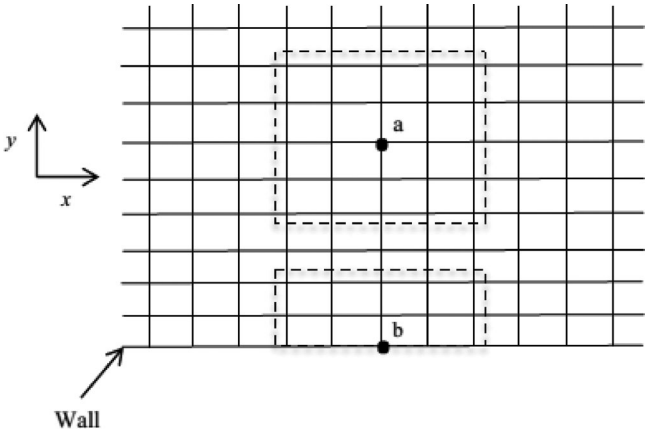

Figure 5. Schematic of the filtering procedure for two specific points ('a' away from the wall and 'b' at the wall), *x*: streamwise, and *y*: wall normal directions. The solid line represents the DNS grid, while the dashed line represents the filter cell.

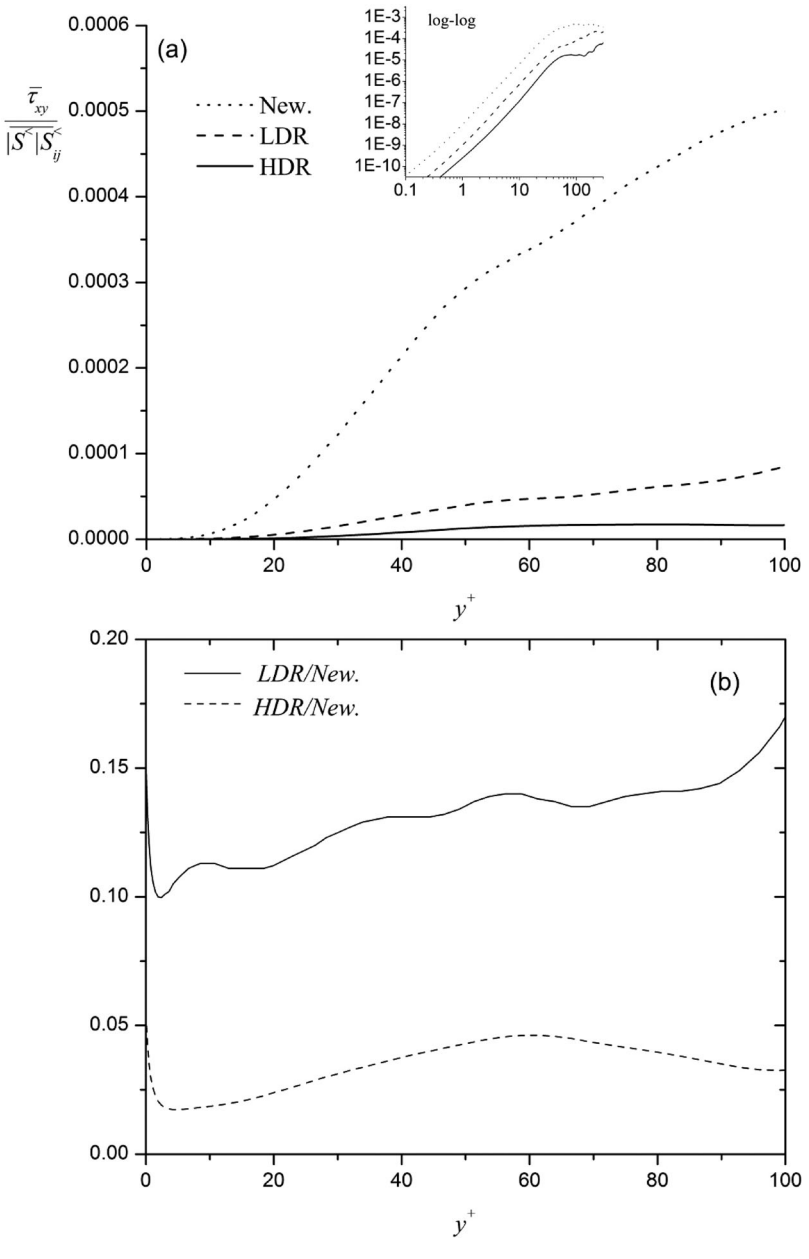

Figure 6. (a) Profiles of $\tau_{xy}/(-S^<_{xy}|S^<|)$ for New., LDR, and HDR cases. (b) Solid line: $(\tau_{xy}/(-S^<_{xy}|S^<|))_{LDR}/(\tau_{xy}/(-S^<_{xy}|S^<|))_{New.}$ and dashed line: $(\tau_{xy}/(-S^<_{xy}|S^<|))_{HDR}/(\tau_{xy}/(-S^<_{xy}|S^<|))_{New.}$. New., LDR, and HDR denote DNS0, DNS1, and DNS2 cases, respectively. The filter size is $4\Delta x$.

to $(C_s\Delta_g)^2$ in LES of Newtonian turbulence, is plotted in Figure 6(a) using the a-priori DNS data for viscoelastic (high drag reduction (HDR): case DNS2 and low drag reduction (LDR): case DNS1) and Newtonian cases. As can be seen, this quantity is severely suppressed by the addition of polymers to the solvent and keeps decreasing for increasing DR. In order to have an idea about the amount of suppression and the overall change in the

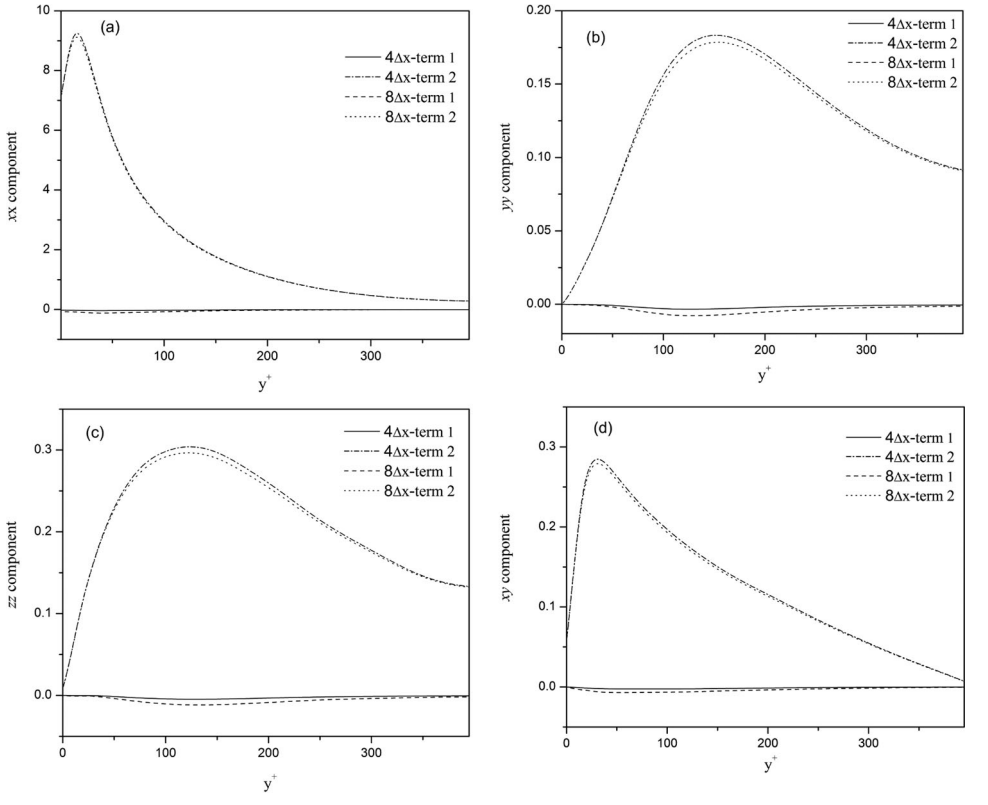

Figure 7. Profiles of components of term 1: $(\eta_p/\lambda)(f(c_{kk})c_{ij})^< - (\eta_p/\lambda)f(c_{kk})^<c_{ij}{}^<$ and term 2: $(\eta_p/\lambda)[f(c_{kk})^<c_{ij}{}^< - f(L)\delta_{ij}]$ for the: (a) streamwise, (b) wall normal, (c) spanwise components, (d) *xy* components of HDR case (DNS2).

shape of this quantity for viscoelastic cases in relation to the Newtonian flow case, the quantities $(\tau_{xy}/(-S^<_{xy}|S^<|))_{\mathrm{LDR}}$ and $(\tau_{xy}/(-S^<_{xy}|S^<|))_{\mathrm{HDR}}$ over $(\tau_{xy}/(-S^<_{xy}|S^<|))_{\mathrm{New.}}$ are plotted in Figure 6(b). It is interesting to note that the ratios are almost constant, with values of about 0.12 for low drag reduction and of 0.03 for high drag reduction regimes, indicating that for FENE-P fluids the overall shape of $(C_s\Delta_g)^2$ remains similar to that for Newtonian fluid, suggesting that a simple extension of the Newtonian closures may be effective to account for the influence of viscoelasticity on the SGS tensor.

Another unknown term that appears in the filtered momentum equation is the filtered viscoelastic stress tensor, which can be split into

$$\tau^<{}_{ij,v} = \underbrace{(\eta_p/\lambda)\left[\left(f(c_{kk})c_{ij}\right)^< - f(c_{kk})^<c_{ij}{}^<\right]}_{\text{term 1}} + \underbrace{(\eta_p/\lambda)\left[f(c_{kk})^<c_{ij}{}^< - f(L)\delta_{ij}\right]}_{\text{term 2}}. \quad (15)$$

In this equation, term 2 is available in the LES grid since it contains only large scale quantities, whereas term 1 involves SGS contributions of the C_{ij} and therefore is unknown in LES. Both terms are compared in Figure 7 for the smallest and largest filter sizes used in this study, and it is clear that regardless of the filter size

in all directions $(\eta_p/\lambda)[(f(c_{kk})c_{ij})^< - f(c_{kk})^< c_{ij}^<]$ is nearly 40 times smaller than $(\eta_p/\lambda)[f(c_{kk})^< c_{ij}^< - f(L)\delta_{ij}]$ indicating that it is possible to safely approximate the filtered viscoelastic extra stress tensor in the filtered Navier–Stokes equation, $\tau^<{}_{ij,v}$, using only its second GS term, i.e.

$$\tau^<{}_{ij,v} \simeq \frac{\eta_p}{\lambda}\left[f(c_{kk})^< c_{ij}^< - f(L)\delta_{ij}\right]. \tag{16}$$

Essentially, this is in agreement with the suppression of small scale turbulence structures in the flow in the presence of polymer additives as observed in Figure 6. In order to shed light on this phenomenon, the visualisation of the coherent structures using the Q criterion ($Q = 1/2(\|\Omega\|^2 - \|S\|^2)$, where Ω and S are the antisymmetric and symmetric parts of ∇u) are shown in Figure 8 for the Newtonian, low, and high drag reduction flow cases. The figure illustrates the dramatic weakening of the flow structures as drag reduction is increased, since it can be observed that the number of vortices is severely reduced with increasing drag reduction. This reduction is particularly significant at the high drag reduction regime, showing smaller number of small scale structures compared to the other cases.

In the filtered conformation tensor equation (Equation 11), there are also two unknown SGS terms, which need to be analysed, terms FT_{ij} and ST_{ij}. FT_{ij} represents the SGS contribution to the advective transport of the filtered conformation tensor by the velocity field, and ST_{ij} represents the SGS contribution from the interaction between the components of the conformation tensor and the velocity gradient tensor, and is originated from the distortion term of the Oldroyd derivative of the filtered conformation tensor. Regardless of the filter size and the amount of drag reduction, it was found that FT_{ij} is almost zero across the channel (see Figure 9), hence the contribution from this term to the filtered conformation tensor can be safely neglected. The trace and xy component of ST_{ij} are also plotted in Figure 9, for the LDR and HDR cases using different filter sizes and are compared with the corresponding GS exact term $(c_{ik}^<\partial u_j^</\partial x_k + c_{jk}^<\partial u_i^</\partial x_k)$. As can be observed, ST_{kk} has a very small magnitude in comparison with $c_{ik}^<\partial u_j^</\partial x_k + c_{jk}^<\partial u_i^</\partial x_k$ and is almost independent of the filter size. On the other hand, its xy component is somehow comparable to $c_{xk}^<\partial u_y^</\partial x_k + c_{yk}^<\partial u_x^</\partial x_k$ especially for larger filter sizes, where ST_{xy} is almost 15% of the corresponding GS term, $(c_{ik}^<\partial u_j^</\partial x_k + c_{jk}^<\partial u_i^</\partial x_k)$. Hence, ST_{ij}, and in particular its shear component, is non-negligible in our point of view especially for high drag reduction regime (it is negligible for low drag reduction case, see Figure 9(d)), where the resolved polymer mean shear stress is comparable to the Reynolds shear stress (see Figure 4(c)). In summary, the term-by-term analysis of the filtered conformation tensor reveals that the filtered conformation equation can be approximated as

$$\frac{\partial c_{ij}^<}{\partial t} + u_k^<\frac{\partial c_{ij}^<}{\partial x_k} - \left(c_{ik}^<\frac{\partial u_j^<}{\partial x_k} + c_{jk}^<\frac{\partial u_i^<}{\partial x_k}\right) + \frac{\tau_{ij,v}^<}{\eta_p} = ST_{ij}. \tag{17}$$

4.2. Analysis of the grid and subgrid-scale interactions

Figures 10(a)–10(g) plot plane-averaged profiles of the various terms in the budget of the SGS kinetic energy transport equation, as a function of the dimensionless wall distance, y^+, for Newtonian and the low and high drag reduction viscoelastic cases (HDR: case DNS2 and LDR: case DNS1). As in all the results presented here, the number of realisations is sufficient

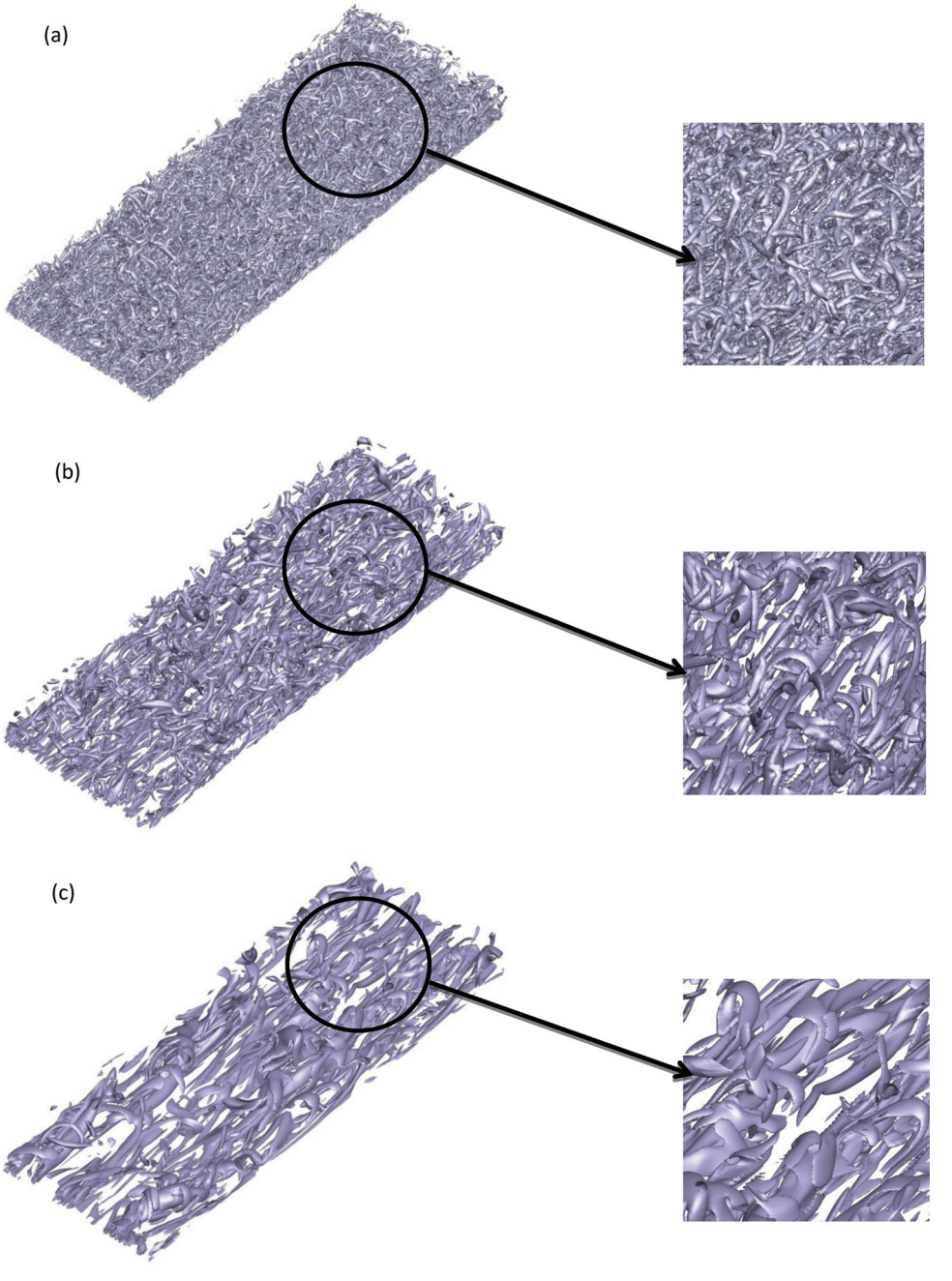

Figure 8. Vortex visualisation through iso-surfaces of $Q > 0$: (a) Newtonian, (b) LDR, and (c) HDR cases. The same threshold was used for all cases.

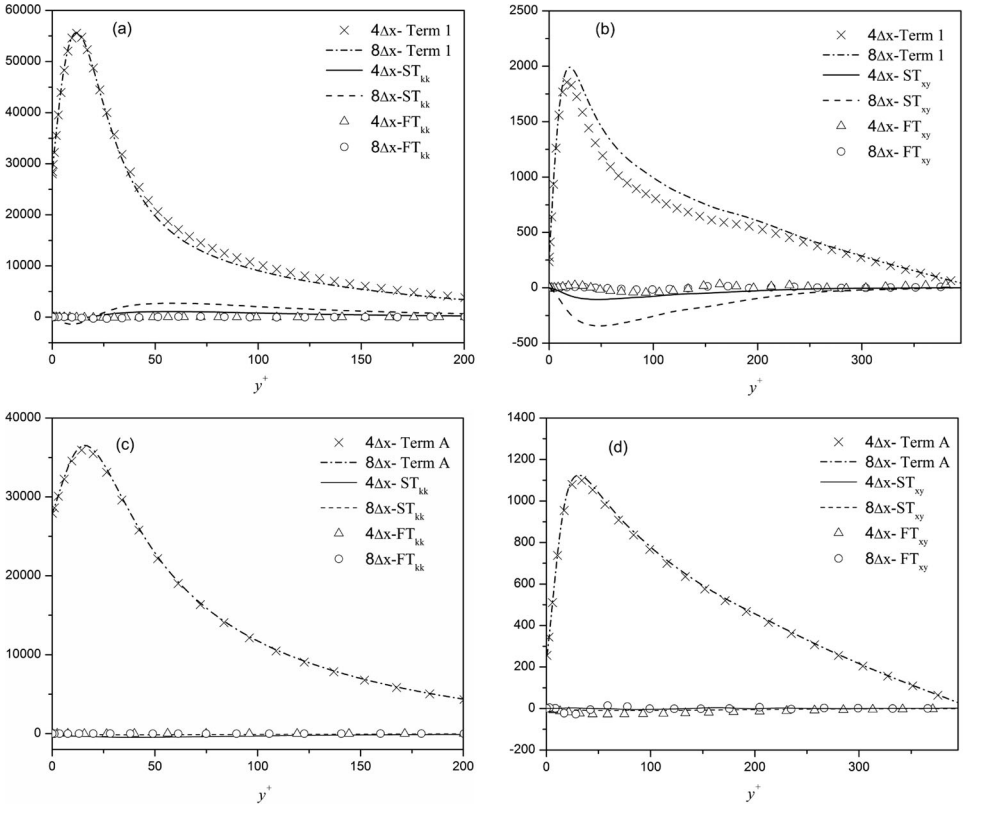

Figure 9. Comparison between FT_{ij}, ST_{ij}, and term A: $(c_{ik}^{<}\partial u_j^{<}/\partial x_k + c_{jk}^{<}\partial u_i^{<}/\partial x_k)$: (a) tensor trace, HDR; (b) *xy* component, HDR; (c) tensor trace, LDR; and (d) *xy* component, LDR.

to converge the budgets. In order to have an idea about the instantaneous behaviour of different terms, the probability density function (PDF) of terms K, L, M, N, O, and P at $y^+ = 5$ and $y^+ = 21$ are plotted in Figure 11(a) and 11(b), respectively.

The advective variation of the SGS kinetic energy, term K, is plotted in Figure 10(a). The magnitude of the maxima is almost constant, and only weakly affected by the presence of the polymers and intensity of DR, although a shift of the peak location can be observed. This shift is consistent with the notion of the expansion of the buffer layer associated with drag reduction by polymer additives.

The terms involving only GS/SGS interactions within the solution, i.e. terms associated with the SGS turbulent transport, SGS pressure/velocity interactions, SGS viscous diffusion, and SGS viscous dissipation are plotted in Figures 10(b)–10(e), respectively. The magnitude of the maxima and minima of all these terms display a pronounced suppression with increasing DR especially close to the wall. The figures show that these quantities for LDR regime decrease by around 60% relative to the Newtonian case, and for HDR case this reduction is around 80%. In addition, a shift farther from the wall of the peak value is observed with increasing DR, which is also conceptually consistent with the notion of the expansion of the buffer layer associated with drag reduction. It can be inferred that these terms show the most significant reduction relative to their Newtonian values and provide

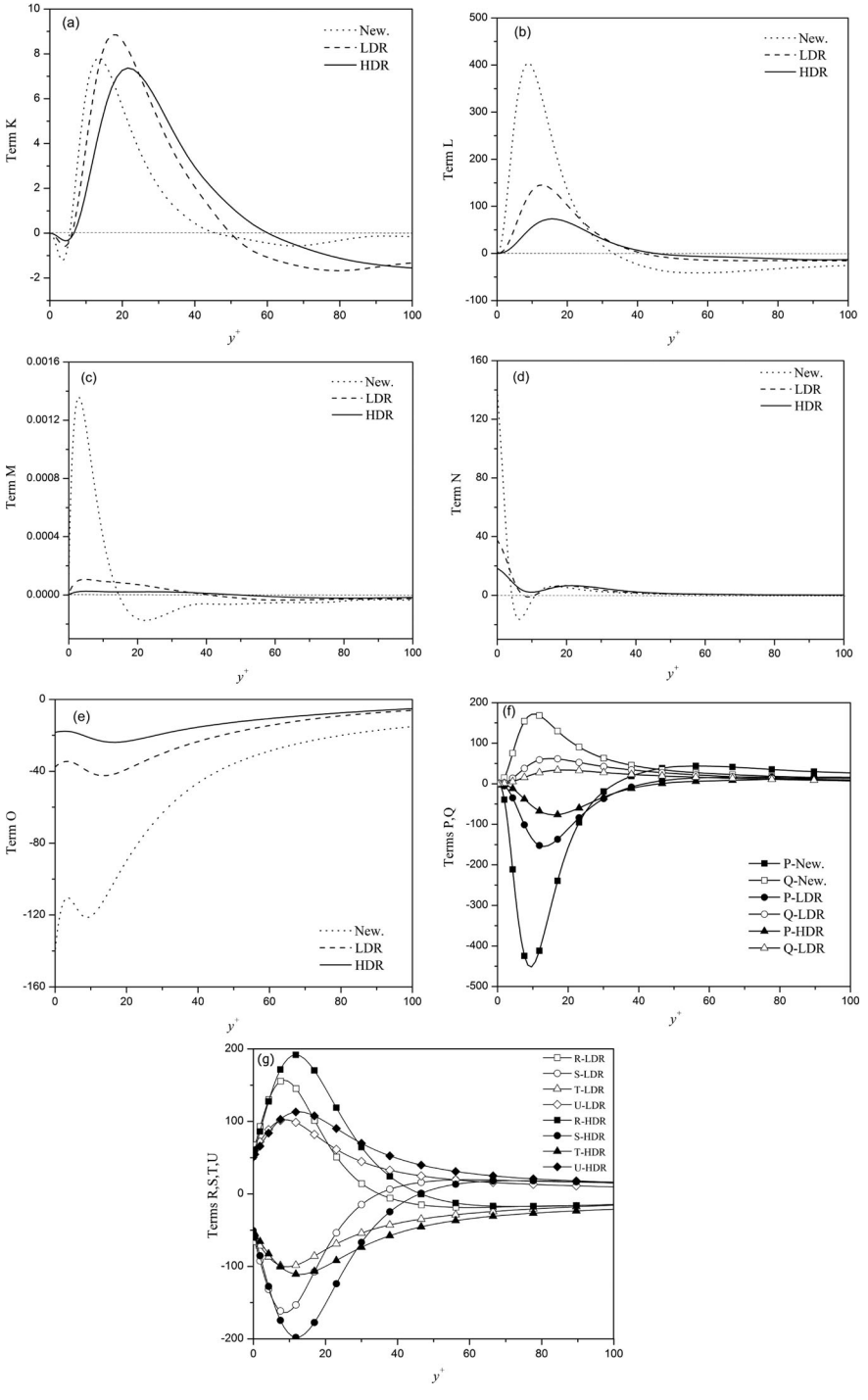

Figure 10. Plane-averaged terms appearing in the SGS transport equation (Equation (13)). New., LDR, and HDR denote DNS0, DNS1, and DNS2 cases, respectively. The filter size is $8\Delta x$. A horizontal dashed line is shown in parts (a)–(d) to separate positive and negative mean values of the terms.

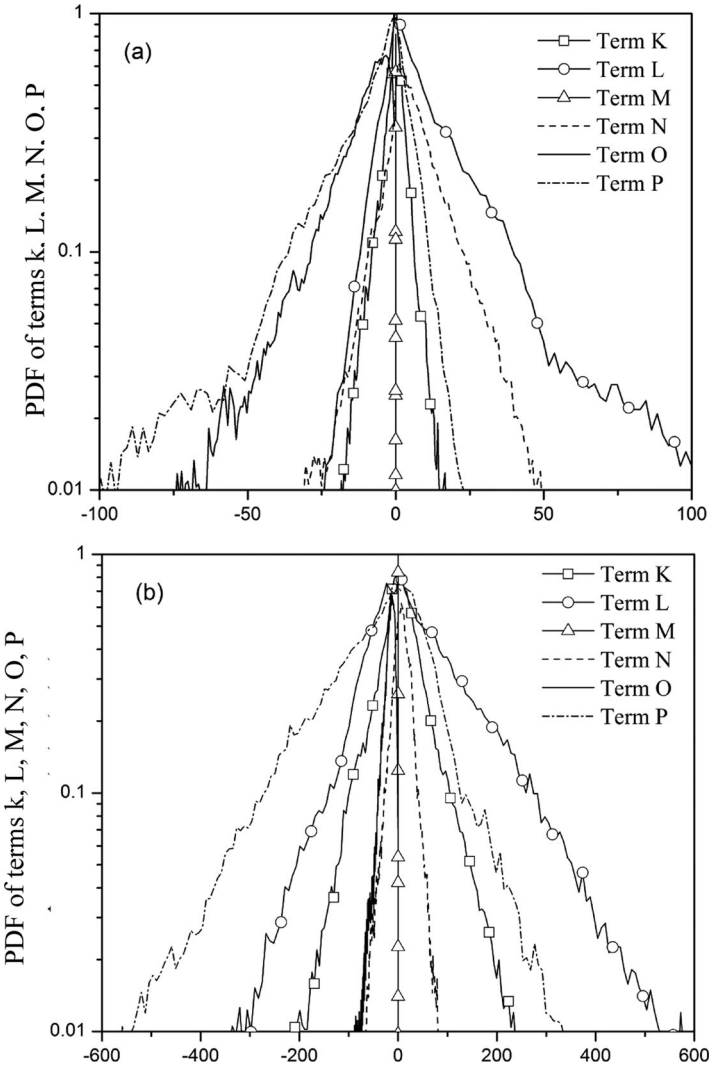

Figure 11. Probability density function of terms K, L, M, N, O, and P, for case HDR (DNS2). The filter size is $8\Delta x$: (a) at $y^+ = 5$ and (b) at $y^+ = 21$.

insight into the effects of polymer additives onto the SGS kinetic energy transport equation. Note that as for the Newtonian fluid, in the viscoelastic cases the advective term as well as all the diffusion-like terms, such as pressure–velocity, viscous, SGS diffusion, and turbulent transport, do not create or destroy energy but only redistribute it between adjoining volumes. The mean classical GS/SGS diffusion and SGS dissipation for the viscoelastic and Newtonian flows are plotted in Figure 10(f). For the HDR case, the peak value of the GS/SGS diffusion has decreased to 30% of the corresponding Newtonian value showing that polymer additives cause a severe reduction in the local energy transfer between the GS and SGS.

Comparing the magnitude of all the terms in Figure 10 shows that term M is less than 1% of the magnitude of other terms for both Newtonian and viscoelastic flows, hence it is

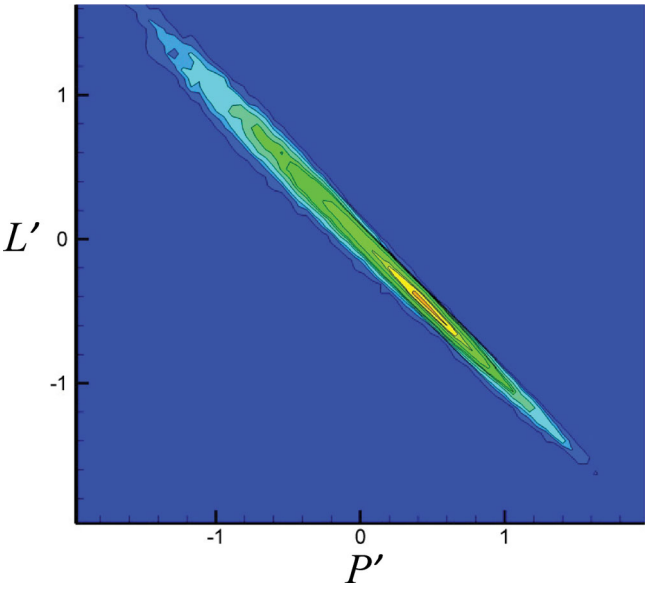

Figure 12. Joint PDF of terms L and P for case HDR (DNS2). The filter size is $8\Delta x$.

negligible in the budgets of SGS transport. This is also confirmed from its PDF depicted in Figure 11(a) and 11(b). The SGS turbulent transport (term L) and SGS diffusion (term P) have a noticeable magnitude in the SGS transport equation. In figure 12 the joint PDF for terms L and P for HDR case is plotted at $y^+ = 17$, the locus of its peak value showing that for all events these quantities are highly correlated for the viscoelastic fluids as it is also for Newtonian fluids (not shown for conciseness). The correlation coefficient for these terms exceeds -98% all across the channel, indicating that terms L and P are in local and statistical equilibrium for viscoelastic cases as for Newtonian. This is important because it shows that for viscoelastic fluids as for Newtonian flows based on the findings of [15], the SGS diffusion, although significant, cancels the turbulent transport term almost exactly. Consequently, as stated in [15] for Newtonian flows, if one wishes to model the SGS kinetic energy transport equation for viscoelastic fluids, the SGS diffusion may be lumped together with the other diffusion terms.

Another classical term that has a noticeable magnitude in the mean SGS kinetic energy transport is the SGS viscous diffusion (term N). Figure 10(d) shows that this term is active very close to the wall and drops to zero at around $y^+ = 10$, regardless of the fluid. Comparing Figures 10(d), 10(e), 11(a), and 11(b) the SGS viscous diffusion (term N) has a similar magnitude, but an opposite sign to the SGS viscous dissipation (term O) at $y^+ < 10$. The joint PDF of both terms at $y^+ = 5$ is shown in Figure 13, indicating that these terms not only in the mean but also instantaneously are highly correlated, their correlation coefficient close to the wall, where the viscous dissipation is more active ($y^+ < 10$), is equal to -90% confirming that almost all the energy produced by term N, dissipates by the SGS viscous dissipation.

The last four terms on the SGS kinetic energy transport equation are the new terms containing the viscoelastic stresses, and are plotted in Figure 10(g). The figure shows that by

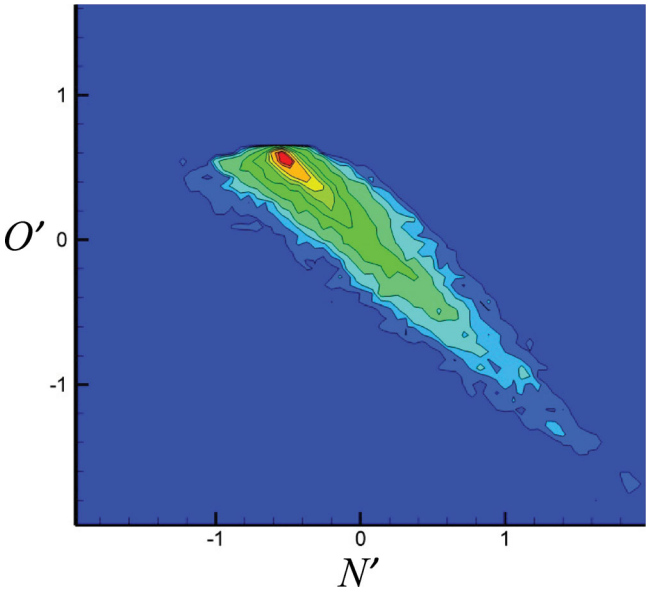

Figure 13. Joint PDF of terms O and N for case HDR (DNS2). The filter size is $8\Delta x$.

increasing DR the peak values associated with these terms display a slight increase, and move away from the wall. The terms R,S and T,U seem to be nearly symmetric in plane-averaged budgets of SGS transport equation. In Figure 14 terms U+T and R+S are plotted, and for the sake of comparison the classical SGS dissipation (term Q) is also included in the figure. The two diffusion-like terms associated with the polymer stresses, terms R

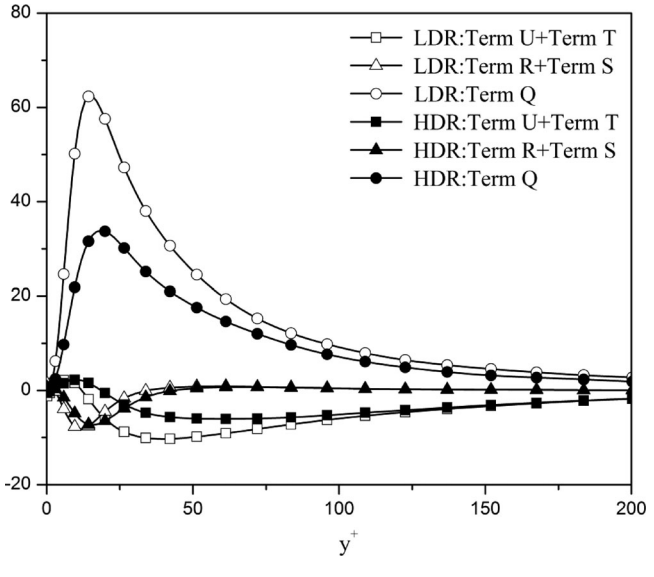

Figure 14. Mean U+T and R+S terms. LDR and HDR denote DNS1 and DNS2, respectively. The filter size is $8\Delta x$.

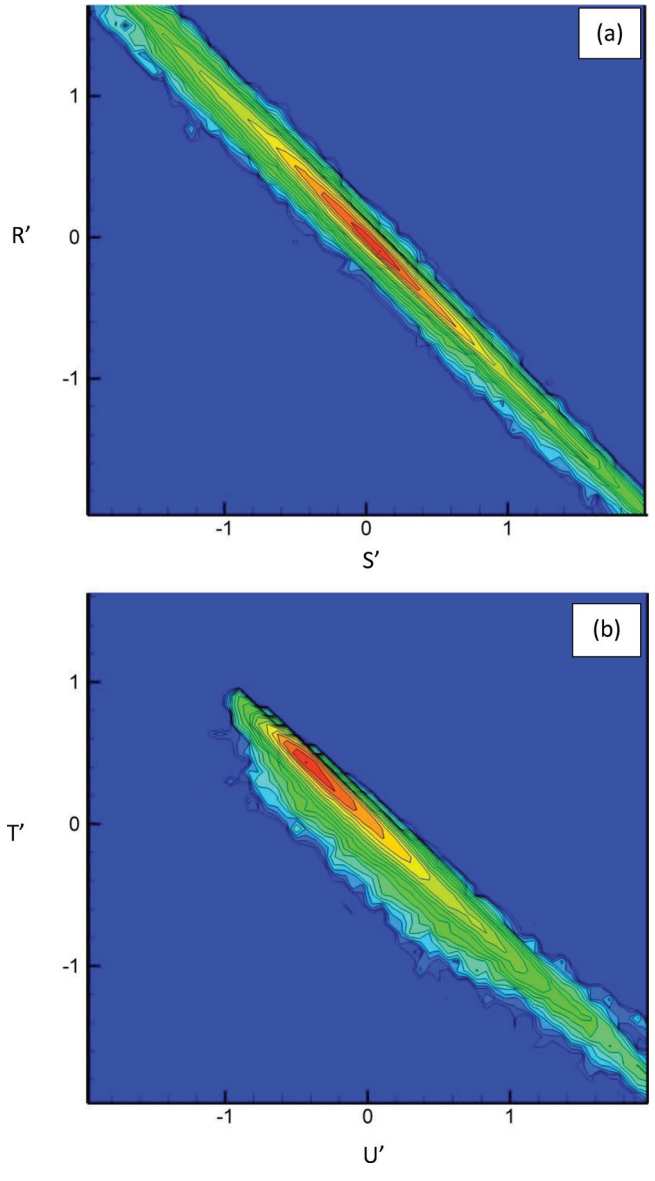

Figure 15. Joint PDF of terms (a): R and S, (b): U and T, for case HDR (DNS2). The filter size is $8\Delta x$.

and S, nearly cancel out across the channel and their sum has a small magnitude in comparison to the SGS dissipation. The same happens for terms T and U close to the wall, for which the figure shows that their sum is very small compared to the SGS dissipation (around 5-15%), however as can be seen, far from the wall, term T+U has same magnitude as term Q. In order to better assess the behaviour of these two pairs of terms, their joint PDFs are plotted at $y^+ = 17$ (the place of its maximum value) for the HDR case (Figure 15), showing that for all events these quantities, U,T and R,S, are highly correlated. Furthermore, the variation across the channel of the correlation coefficient for terms R,S and for

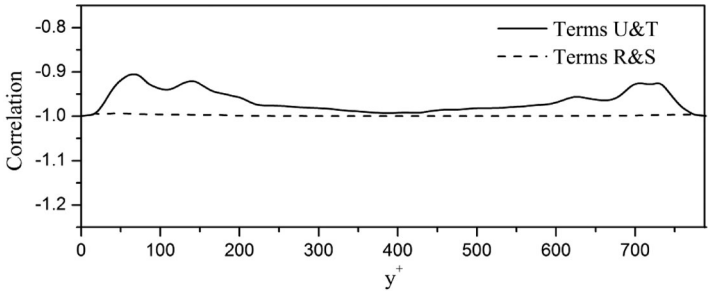

Figure 16. Correlation coefficient of terms U,T and R,S for case HDR (DNS2). The filter size is $8\Delta x$.

terms T, U are calculated using the instantaneous field data for the largest filter size and the plane-averaged correlation is plotted in Figure 16. The figure shows that terms R and S are highly correlated (their correlation coefficient is above −99%), whereas the plane-averaged correlation coefficient for terms T and U varies between −99% to −90% stating that although they are highly correlated for all events, some part of kinetic energy induced by the polymer plays a small role in the budget of SGS kinetic energy transport equation.

In summary, although term T+U has a noticeable magnitude far from the wall, each pair of the new viscoelastic terms U, T and R,S, are in local and statistical equilibrium. Concerning the relevance (in terms of the mean and instantaneous values) of the terms for the SGS kinetic energy transport equation in turbulent channel flow of FENE-P fluids, the most important terms are the classical SGS viscous diffusion (term N),viscous dissipation (term O), and SGS dissipation (term Q). On the other hand, when taken together several other terms investigated cancel each other, e.g. terms P, L, R, S, or have small magnitudes, e.g. term M. These observations suggest that the SGS kinetic energy transport equation for viscoelastic fluids can be well approximated by the following relationship:

$$\underbrace{\frac{\partial \tau_{ii}}{\partial t}}_{(J)} + \underbrace{\frac{\partial \tau_{ii} u_j^{<}}{\partial x_j}}_{(K)} \simeq \underbrace{\frac{\beta}{\mathrm{Re}_\tau}\frac{\partial}{\partial x_j}\left(\frac{\partial \tau_{ii}}{\partial x_j}\right)}_{(N)} \underbrace{-\frac{2\beta}{\mathrm{Re}_\tau}\left(\left(\frac{\partial u_i}{\partial x_j}\frac{\partial u_i}{\partial x_j}\right)^{<} - \frac{\partial u_i^{<}}{\partial x_j}\frac{\partial u_i^{<}}{\partial x_j}\right)}_{(O)} \underbrace{-2\tau_{ij}S_{ij}^{<}}_{(Q)}$$
$$\underbrace{-2(1-\beta)\left(\tau_{v,ij}S_{ij}\right)^{<}}_{(T)} + \underbrace{2(1-\beta)\tau_{v,ij}^{<}S_{ij}^{<}}_{(U)}. \tag{18}$$

This equation could be used as a starting point in the development of LES closures for viscoelastic fluids, similar to LES approaches based on SGS energy equations, e.g.[24]

4.3. Influence of viscoelasticity on kinetic energy inverse transfer or backscatter

The interaction between resolved and unresolved scales through the SGS dissipation (term Q) has received much attention in Newtonian turbulent flow.[15–17] In this section, the influence of polymer additives on the kinetic energy transfer (backward as well as forward scatter) is investigated by analysing the SGS dissipation in more detail. The PDF of the SGS dissipation at $y^+ = 30$ (i.e. at the peak of turbulent kinetic energy) is plotted for the low and high drag reduction cases along with the Newtonian case in Figure 17. It can be observed that although the forward scatter dominates for all flows in the near wall region,

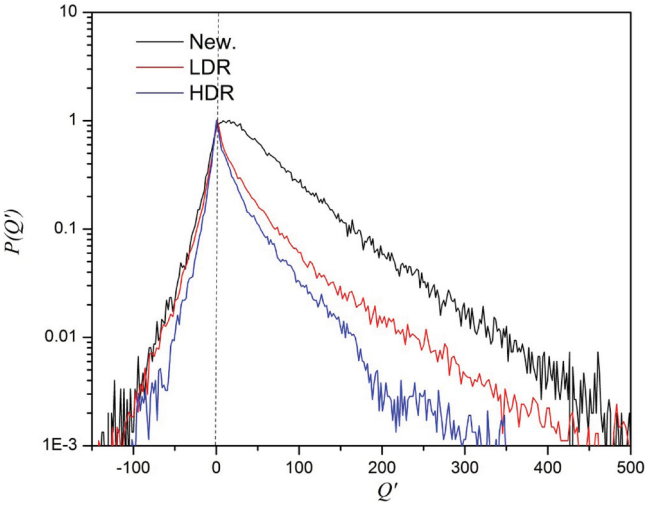

Figure 17. PDF of the SGS dissipation (term Q). New., LDR, and HDR denote DNS0, DNS1, and DNS2, respectively. The filter size is $8\Delta x$.

the increase in drag reduction severely reduces these events while leaving the backscatter tail nearly unchanged. Hence, this implies that backscatter of SGS dissipation is relatively more important for viscoelastic flows than for Newtonian flows particularly for high drag reduction regimes. This can be observed also in the instantaneous field data plotted for Newtonian and viscoelastic cases in Figure 18. In order to investigate this, the backward

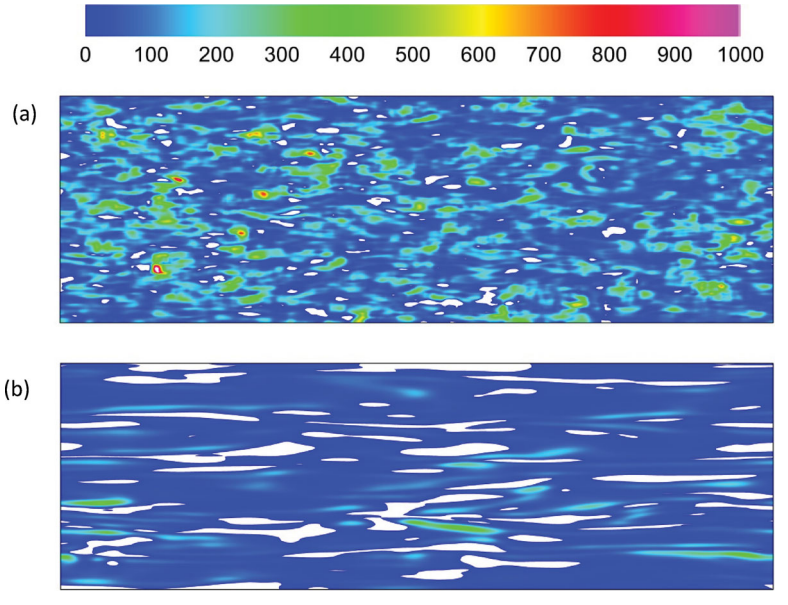

Figure 18. Contours of the SGS dissipation (term Q). (a) Newtonian and (b) HDR, case DNS2. The filter size is $8\Delta x$. White spots are backward scatter events.

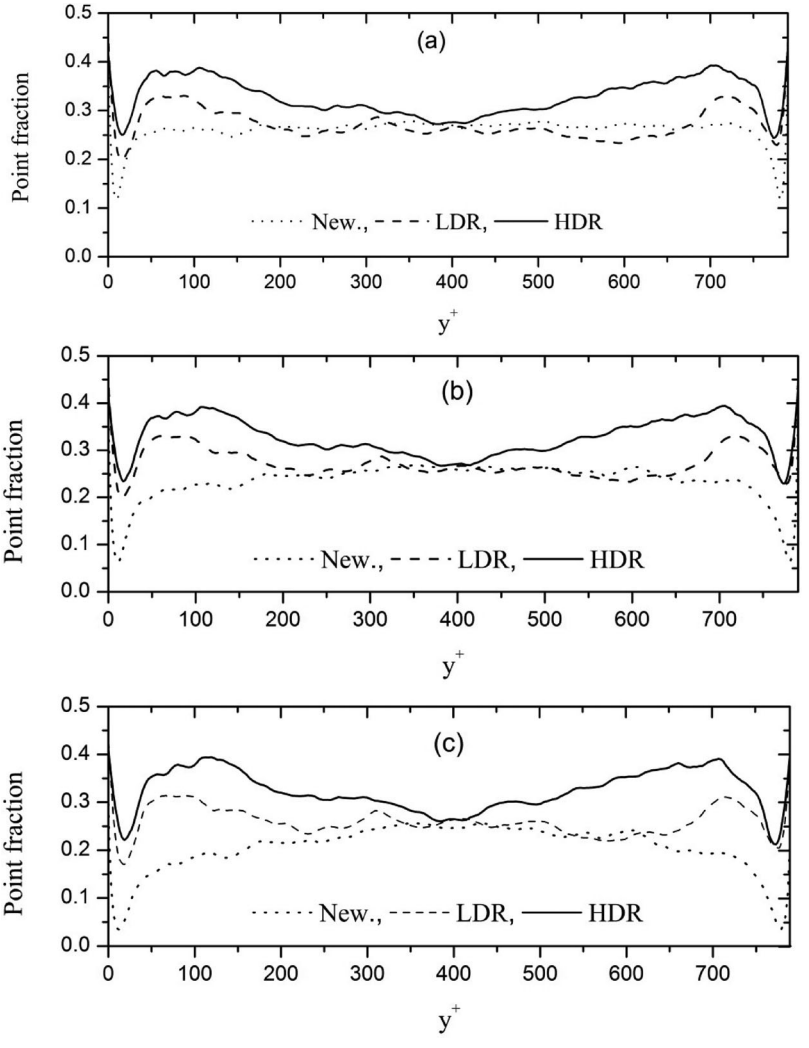

Figure 19. Fraction of points with backward scatter events for the filter sizes defined as (a) $4\Delta x$, (b) $6\Delta x$, and (c) $8\Delta x$. New., LDR, and HDR denote DNS0, DNS1, and DNS2, respectively.

and forward scatter part of ε_{SGS} are quantified as

$$\varepsilon^- = \frac{1}{2}(\varepsilon_{SGS} - |\varepsilon_{SGS}|)\,, \quad \varepsilon^+ = \frac{1}{2}(\varepsilon_{SGS} + |\varepsilon_{SGS}|), \tag{19}$$

where ε^- and ε^+ denote backward and forward scatter contributions to the SGS dissipation, respectively. Using this definition, the fraction of points with backward scatter events (ratio of computational cells experiencing backward scatter in each wall normal plane over the total number of cells in the plane) are calculated and plotted in Figure 19 across the channel for the three simulations and for the three filter sizes. The figure shows that the backward scatter is almost independent of grid size (the maximum variation caused by the filter size is around ±5%), similarly to what is observed for Newtonian channel flows.[15,16]

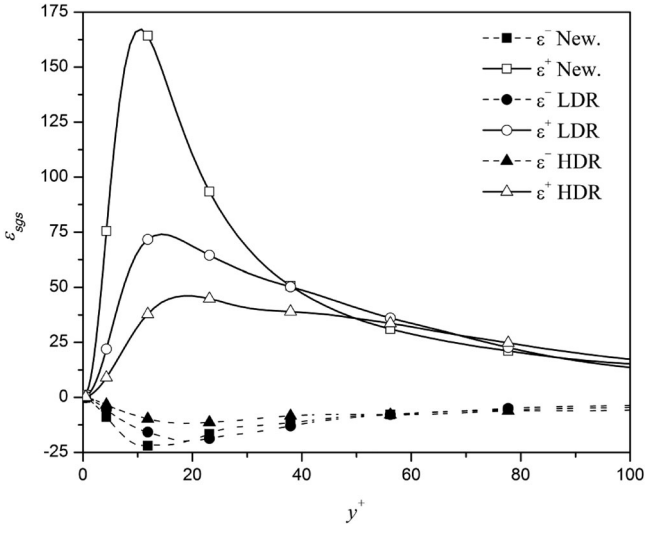

Figure 20. Mean backward and forward scatter of SGS dissipation. New., LDR, and HDR denote DNS0, DNS1, and DNS2 cases, respectively. The filter size is $8\Delta x$.

Moreover, Figure 19 indicates that the fraction of points experiencing the backward scatter increases (in the mean) with the addition of polymer to the fluid. Regardless of the filter size the average number of points/events experiencing backward scatter across the channel is 24%, 31%, and 35% for the Newtonian, LDR and HDR flows, respectively. The intensity of the plane-averaged forward and backward scatter contributions to SGS dissipation computed by Equation (19) is plotted in Figure 20 for the three flow cases. We observe a severe decrease in forward scatter as drag reduction increases, although it remains more important than backscatter. Conceptually, this severe reduction of forward scatter events is in agreement with the suppression and laminarisation of turbulence structures by the addition of polymers to the carrier flow, as previously shown in Figure 8, i.e. as also seen in Figure 10(f) (plane-averaged SGS dissipation), the total amount of SGS dissipation events is severely reduced with increasing DR, hence the instantaneous intensity of energy transfer between GS and SGS is dramatically reduced. The figure further indicates that the ratio of backward scatter to forward scatter nearly doubles with enhancing drag reduction, and at the peak location this ratio is 0.15, 0.24, and 0.27 for the Newtonian, LDR, and HDR flows, respectively. In summary, Figures 18 and 19 indicate that not only the number of backward scatter events increases by the addition of polymer to the flow, but also the intensity of the backward scatter events increases in relation to the forward scatter.

As mentioned before, the dissipation term prompted by the polymer (term U) is also responsible (indirectly) for the net kinetic energy exchange between resolved and unresolved scales. In order to investigate this specific mechanism the PDF of this term close to the wall ($y^+ = 30$) is plotted in Figure 21, showing that this viscoelastic term is mostly responsible for forward scatter. This is also confirmed by the fraction of points experiencing backward scatter due to the polymer induced dissipation, plotted in Figure 22. This figure shows that similarly as for the SGS dissipation, the polymer induced indirect backward scatter is almost independent of the filter size. Furthermore, close to the wall only 2% of the

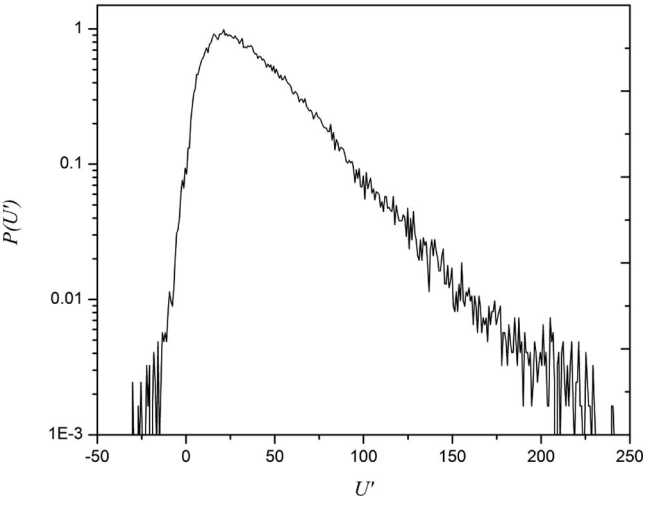

Figure 21. PDF of the term U for case HDR (DNS2). The filter size is $8\Delta x$.

points are experiencing polymer induced backward scatter with the maximum at the channel centreline region which is around 10%, i.e. backward scatter events due to the polymer induced dissipation are rare. Finally, iso-surfaces of the backward scatter of the dissipation prompted by the polymer along with forward and backward scatter of classical SGS dissipation for the HDR case are plotted in Figure 23. The figure shows that backward and forward scatter events of the SGS dissipation in turbulent viscoelastic fluids usually occur in close proximity to each other, with the backscatter event being generally surrounded by a

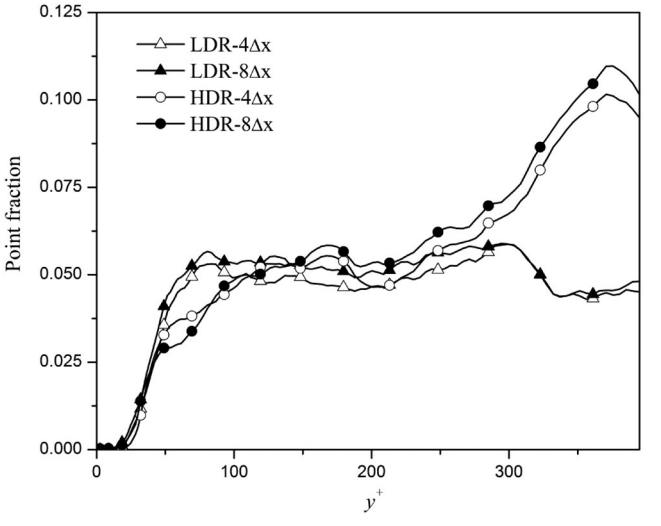

Figure 22. Fraction of points experiencing backward scatter due to the polymer induced dissipation. LDR and HDR denote DNS1 and DNS2, respectively.

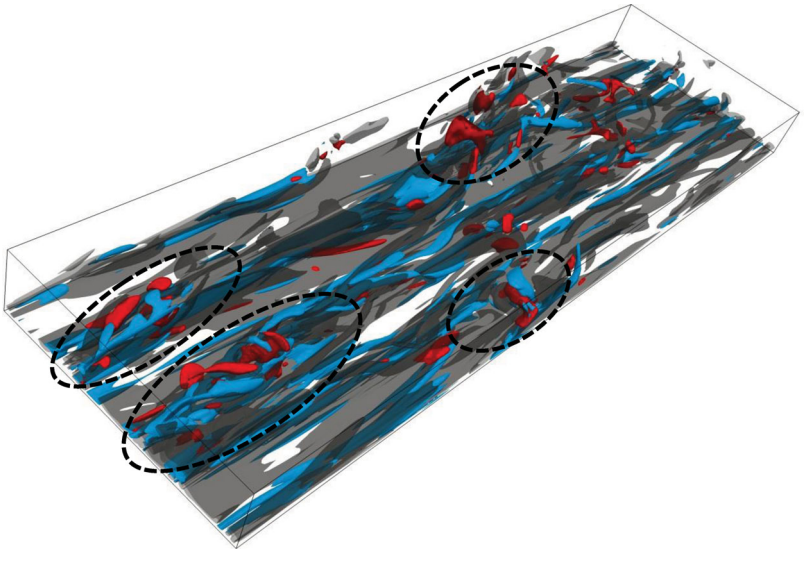

Figure 23. Iso-surface of backward (light grey/blue), forward (dark grey/black) scatter of SGS dissipation, and of backward scatter of term U (medium grey/Red), using a filter size of $\Delta = 4\Delta x$ for case DNS2.

region of significant forward scatter, as previously reported by Piomelli et al. [16] for Newtonian fluids. Figure 23 also confirms that backward scatter events associated with polymer-induced SGS dissipation are very rare in comparison with the backward and forward scatter events of the SGS dissipation. Moreover it is interesting to note that the polymer induced backscatter event of dissipation also takes place in close proximity to backward and forward scatter events generated by the SGS dissipation (they are surrounded by a region of significant forward and backward scatter events of SGS dissipation). These regions are shown in Figure 23 using dashed circles (Note that equal thresholds were chosen to illustrate iso-surfaces of the various quantities).

5. Conclusion

The main goal of this work was to understand how the grid/subgrid-scale interactions are affected by the presence of the polymer additives in turbulent channel flow. This was achieved by the application of the top-hat filter to DNSs of channel flow of viscoelastic fluids described by the FENE-P rheological constitutive equation. The influence of rheological parameters on the SGS stress tensor show that in the presence of polymer additives the SGS stresses are considerably reduced compared to the Newtonian case. The ratio $\tau_{xy}/(-S^{<}_{xy}|S^{<}|)$, which is equal to $(C_s\Delta_g)^2$, the key parameter in classical closures for LES, was analysed and it was observed that although this quantity severely decreases for viscoelastic fluids, the overall shape and behaviour remains proportional to that for Newtonian fluids, and the ratio of this quantity for viscoelastic case and Newtonian fluid is almost constant, which is a useful result for future attempts to develop SGS modes for viscoelastic fluids.

The exact filtered polymer extra stress tensor arising in the filtered Navier–Stokes equation shows that even for high drag reduction cases with the largest filter size this term

can be safely approximated by its large-scale contribution and does not require modelling. The filtered evolution equation for the conformation tensor was also inspected in detail and an approximated form was introduced after a quantitative assessment of its GS/SGS terms.

The energy transfer between grid scales, subgrid scales, and polymer in the SGS kinetic energy transport equation appropriate for the FENE-P fluids was investigated. The budgets for Newtonian, low, and high drag reduction cases exhibit a severe suppression of some GS/SGS terms for the viscoelastic cases. It was also found that new terms appearing in this equation due to the presence of polymer additives (SGS/polymer interactions) are almost symmetric, and highly correlated, hence an approximated SGS kinetic energy transport equation was suggested for viscoelastic turbulent flows, which can be used to develop new SGS models based on the SGS kinetic energy transport equation models.[24,25]

Additionally, it was shown that the amount of points in the flow domain experiencing backward scatter events of the SGS dissipation is almost independent of the filter size for viscoelastic turbulent flows as for Newtonian fluids.[15] Moreover, it was observed that the amount of forward scatter events of SGS dissipation in the flow domain decreases significantly in the presence of polymer additives, indicating that backward scatter of SGS dissipation in viscoelastic fluids is proportionally more frequent than in Newtonian fluids and requires attention. Polymer induced dissipation, which is a polymeric term involved in GS/Polymer/SGS energy transfer via GS/polymer and SGS/polymer interactions, causes a very small amount of energy backward scatter, which is negligibly small close to the wall.

Finally, it was found that as for Newtonian fluids,[16] backward and forward scatter events of SGS dissipation for viscoelastic fluids occur in close proximity of each other, with the backward scatter event being generally surrounded by a region of significant forward scatter. Rather surprisingly, it was also observed that the backward scatter events associated to the polymer induced dissipation, although very small, occur in close proximity of the backward and forward scatter events generated by SGS dissipation.

Acknowledgements

The authors are grateful to FCT funding via project PTDC/EME-MFE/113589/2009. M. Masoudian and F.T. Pinho also wish to acknowledge funding by FEDER for funding through Programa Operacional do Norte (ON2) and for National funds of FCT/MEC (PIDDAC) via project NORTE-07-0124-FEDER-000026. M. Masoudian acknowledges LASEF members and especially Dr Pedro Valente at IST for their hospitality and scientific discussions C.B. da Silva.

Disclosure statement

No potential conflict of interest was reported by the authors.

Funding

The authors are grateful to FCT funding via project PTDC/EME-MFE/113589/2009. M. Masoudian and F.T. Pinho also wish to acknowledge funding by FEDER through Programa Operacional do Norte (ON2) and for National funds of FCT/MEC (PIDDAC) via project NORTE-07-0124-FEDER-000026, and Fundação para a Ciência e a Tecnologia (FCT), through IDMEC, under LAETA, project UID/EMS/50022/2013.

References

[1] Toms BA. Observation on the flow of linear polymer solutions through straight tubes at large Reynolds numbers. Proceedings of the International Rheological Congress, vol. 9. Holland; 1949.

[2] Dimitropoulos CD, Sureshkumar R, Beris AN. Direct numerical simulation of viscoelastic turbulent channel flow exhibiting drag reduction: effect of the variation of rheological parameters. J Non-Newton Fluid Mech. 1998;79:433–468.

[3] Kawaguchi Y, Segawa T, Feng ZP, et al. Experimental study on drag-reducing channel flow with surfactant additives spatial structure of turbulence investigated by PIV system. Int J Heat Fluid Flow. 2002;23(5):700–709.

[4] Dubief Y, White CM, Terrapon VE, et al. On the coherent drag reducing and turbulence enhancing behavior of polymers in wall flows. J Fluid Mech. 2004;514:271–280.

[5] Vaithianathan T, Collins LR. Numerical approach to simulating turbulent flow of a viscoelastic polymer solution. J Comp Phys. 2003;187(1):1–21.

[6] Lumley JL. Drag reduction by additives. Annu Rev Fluid Mech. 1969;1:367–384.

[7] Tabor M, de Gennes PG. A cascade theory of drag reduction. Europhys Lett. 1986;2:519–522.

[8] Li CF, Sureshkumar R, Khomami B. Influence of rheological parameters on polymer induced turbulent drag reduction. J Non-Newton Fluid Mech. 2006;140:23–40.

[9] Kawaguchi Y, Wei JJ, Yu B, et al. Rheological characterization of drag-reducing cationic surfactant solution shear and elongational viscosities of dilute solutions. Proceedings of the Fluids Engineering Division Summer Meeting; 2003 Jul 1; Honolulu. ASME/JSME, DOI 10.1115FEDSM2003-45653.

[10] Iaccarino G, Shaqfeh ESG, Dubief Y. Reynolds-averaged modeling of polymer drag reduction in turbulent flows. J Non-Newton Fluid Mech. 2010;165:376–384.

[11] Masoudian M, Kim K, Pinho FT, et al. A viscoelastic k-ε-$\overline{v^2}$-f turbulent flow model valid up to the maximum drag reduction limit. J Non-Newton Fluid Mech. 2013;202;99–111.

[12] Thais L, Tejada-Martínez AE, Gatski TB, et al. Temporal large eddy simulations of turbulent viscoelastic drag reduction flows. Phys Fluids. 2010;22:013103.

[13] Wang L, Cai WH, Li F-C. Large-eddy simulations of a forced homogeneous isotropic turbulence with polymer additives. Chin Phys B. 2014;23(3):034701.

[14] Ohta T, Miyashita M. DNS and LES with an extended Smagorinsky model for wall turbulence in non-Newtonian viscous fluids. J Non-Newton Fluid Mech. 2014;206:29–39.

[15] Piomelli U, Cabot WH, Moin P, et al. Subgrid-scale backscatter in turbulent and transitional flows. Phys Fluids. 1991;3:1766–1771.

[16] Piomelli U, Yu Y, Adrian RJ. Subgrid-scale energy transfer and near-wall turbulence structure. Phys Fluids. 1996;8:215–224.

[17] da Silva CB, M´ etais O. On the influence of coherent structures upon inter-scale interactions in turbulent plane jets. J Fluid Mech. 2002;473(1):103–145.

[18] Sureshkumar R, Beris AN, Handler RA. Direct numerical simulation of the turbulent channel flow of a polymer solution. Phys Fluids. 1997;9:743–755.

[19] Masoudian M, Kim K, Pinho FT, et al. A Reynolds stress model for turbulent flow of homogeneous polymer solutions. Int J Heat Fluid Flow. 2015;54:220–235.

[20] Thais L, Gatski TB, Mompean G. Analysis of polymer drag reduction mechanisms from energy budgets. Int J Heat Fluid Flow. 2013;43:52–61.

[21] Thais L, Gatski TB, Mompean G. Some dynamical features of the turbulent flow of a viscoelastic fluid for reduced drag. J Turbulence. 2012;13:1–26.

[22] Virk PS. Drag reduction fundamentals. AIChE J. 1975;21.4:625–656.

[23] Ptasinski PK, Boersma BJ, Nieuwstadt FTM, et al. Turbulent channel flow near maximum drag reduction: simulations, experiments and mechanisms. J Fluid Mech. 2003;490:251–291.

[24] Fureby C, Tabor G, Weller HG, et al. Differential subgrid stress models in large eddy simulations. Phys Fluids (1994-present). 1997;9(11):3578–3580.

[25] Davidson L. Large eddy simulation: a dynamic one-equation subgrid model for three-dimensional recirculating flow. 11th International Symposium on Turbulent Shear Flow, vol. 3; Grenoble. 1997. p. 36. 1–26.6.